SHROOM3 is downstream of the planar cell polarity pathway and loss-of-function results in congenital heart defects

Matthew D. Durbin[a], James O'Kane[a], Samuel Lorentz[b], Anthony B. Firulli[b], Stephanie M. Ware[b,c,*]

[a]Department of Pediatrics, Division of Neonatal-Perinatal Medicine, Indiana University School of Medicine, Indianapolis, IN

[b]Department of Pediatrics, Herman B Wells Center for Pediatric Research, Indiana University School of Medicine, Indianapolis, IN

[c]Department of Medical and Molecular Genetics, Indiana University School of Medicine, Indianapolis, IN

Abstract

Congenital heart disease (CHD) is the most common birth defect, and the leading cause of death due to birth defects, yet causative molecular mechanisms remain mostly unknown. We previously implicated a novel CHD candidate gene, *SHROOM3*, in a patient with CHD. Using a *Shroom3* gene trap knockout mouse (*Shroom3$^{gt/gt}$*) we demonstrate that SHROOM3 is downstream of the noncanonical Wnt planar cell polarity signaling pathway (PCP) and loss-of-function causes cardiac defects. We demonstrate *Shroom3* expression within cardiomyocytes of the ventricles and interventricular septum from E10.5 onward, as well as within cardiac neural crest cells and second heart field cells that populate the cardiac outflow tract. We demonstrate that *Shroom3$^{gt/gt}$* mice exhibit variable penetrance of a spectrum of CHDs that include ventricular septal defects, double outlet right ventricle, and thin left ventricular myocardium. This CHD spectrum phenocopies what is observed with disrupted PCP. We show that during cardiac development SHROOM3 interacts physically and genetically with, and is downstream of, key PCP signaling component *Dishevelled* 2. Within *Shroom3$^{gt/gt}$* hearts we demonstrate disrupted terminal PCP components, actomyosin cytoskeleton, cardiomyocyte polarity, organization, proliferation and morphology. Together, these data demonstrate SHROOM3 functions during cardiac development as an actomyosin cytoskeleton effector downstream of PCP signaling, revealing SHROOM3's novel role in cardiac development and CHD.

*Correspondence to: stware@iu.edu, Address: Herman B Wells Center for Pediatric Research, 1044 W. Walnut, R4 227, Indianapolis, IN. 46202-5225, Phone: 317-278-2807, Fax: 317-274-8679.

Availability of data and materials

All data generated or analyzed during this study are included in this manuscript

Conflicts of interest

The authors declare no conflict of interest.

Introduction

Congenital heart disease (CHD) is the most common cause of death due to birth defects. Despite its frequency, the etiologies remain mostly unknown[1,2]. CHD often results from defective signaling pathways and cell cytoarchitecture. In a previous study, we identified a novel CHD candidate gene, *SHROOM3*, whose encoded protein is associated with the non-canonical Wnt/planar cell polarity (PCP) signaling pathway and the actomyosin cytoskeleton[3,4]. Though unexplored in CHD, SHROOM3 pathogenesis has been studied in other organ systems in both humans and animal models. In humans, *SHROOM3* variants are associated with neural tube defects and kidney disease[5–8]. In animal models, *Shroom3^{gt/gt}* mice exhibit fully penetrant neural tube defects in addition to partially penetrant renal podocyte, thyroid, eye lens placode, and gut tube defects[9–12].

There are four SHROOM proteins, SHROOM1-4, that are characterized by inclusion of one or more of three domains: an extracellular PDZ domain, an actin cyotskeleton binding domain (termed apical protein *Xenopus*/Shroom domain 1, or ASD1), and a domain termed ASD2, that faciliates F-Actin and Myosin II constriction[4,13–15]; SHROOM3 contains all three of these domains. SHROOM3 also contains a C-terminal domain that interacts with Rho-associated protein kinase 1 (ROCK1). The SHROOM3-ROCK1 complexes localize to the cellular apical membrane, facilitating the phosphorylation of myosin and localized actomyosin constriction that alters cell shape[13,16].

Recent evidence places SHROOM3 within the PCP signaling pathway. SHROOM3 interacts with two key components of the PCP signaling pathway, ROCK1[16] and Dishevelled2 (DVL2)[17], and is required for planar polarity[18]. PCP drives developmental processes by altering the actomyosin cytoskeleton[19], and SHROOM3's mechanism also invovles the actomyosin cytoskeleton[4]. *Shroom3* loss-of-function leads to completely penetrant neural tube defects, phenocopying PCP disruption[4]. Collectively, these data suggest that SHROOM3 may serve as an important link between PCP signaling and actomyosin.

PCP establishes apicobasilar polarity in epitheilial sheets and mesenchymal tissues[19–21]. PCP influences multiples stages of cardiac development, so knockout models display a wide range, but characteristic pattern, of CHD lesions[19–21]. Given that PCP drives convergent extension within migrating neural crest[22–26] and second heart field cells[27,28] to the outflow tract (OFT) and ventricles, dysfunction in PCP is most strongly associated with OFT and ventricular anomalies. In mice, disrupting different PCP proteins leads to a similar, characteristic phenotype, including OFT anomalies, membranous ventricular septal defects (VSD) and double outlet right ventricle (DORV)[25,26,29–36]. Later in development, PCP is implicated in ventricular maturation and myocardial polarization, and knockout leads to ventricular thinning with immature and disorganized cardiomyocytes resembling left ventricular noncompaction cardiomyopathy (LVNC)[30,32,37,38]. Early CHD studies focused

on core PCP proteins, including DVL2, however, recent studies demonstrate similar CHD phenotypes after disrupting PCP's Actomyosin terminal effectors, including ROCK1, Ras-related C3 botulinum toxin substrate 1 (RAC1) and Disheveled Associated Activator of Morphogenesis 1 (DAAM1)[28,38,39].

Independent lines of evidence suggest that SHROOM3 function within the PCP pathway may be required for normal cardiac development. We previously identified a *SHROOM3* variant in a patient with a PCP related CHD phenotype[3]. Also, a recent study in zebrafish demonstrates that PCP signaling drives apical actomyosin constriction causing cardiac OFT looping and chamber ballooning[40], and SHROOM3 is necessary for similar apical actomyosin constriction required for neural tube, gut, kidney, and lens development[6,9–12,14].

Here, we establish *Shroom3* as a novel cause of CHD in mice and demonstrate its role downstream of PCP as a terminal actomyosin effector within the heart. Utilizing *Shroom3*$^{gt/gt}$ mice we demonstrate that *Shroom3* is expressed within cardiomyocytes and neural cest cells during important stages of cardiac development. We demonstrate that *Shroom3* loss-of-function leads to cardiac defects in addition to disrupted cardiomyocyte polarity, organization, proliferation and maturity. This study reveals that SHROOM3 provides a new path for PCP signaling to modulate the cytoarchitecture within the heart during cardiogenesis.

Materials and Methods

Mice

Shroom3 heterozygous (Shroom3$^{+/gt),}$ Sox2-Cre, and Dvl2$^{flox/flox}$ mice were obtained from Jackson Laboratory (Bar Harbor, Maine). Genotyping was performed using polymerase chain reaction (PCR) with genomic DNA extracted from ear punches, embryonic tail or yolk sacs. *Shroom3* genotyping was performed using PCR for β-galactosidase (5′-AACTTAATCGCCTTGCAGCA-3′) and (5′-GTAACCGTGCATCTGCCAGT-3′) and all *Shroom3* genotyping was confirmed using real time PCR (RT-qPCR) by Transnetyx (Cordova, TN). For *Dvl2* mice, PCR genotyping was performed as previously described[41]. All mouse experiments were carried out in the Indiana University School of Medicine Animal Resource Center which is accredited by the American Association for Accreditation of Laboratory Animal Care. Animals are maintained in accordance with the applicable portions of the Animal Welfare act and the DHHS Guide for the Care and Use of Laboratory Animals. All studies were approved by the institutional animal care and use committee (IACUC).

X-gal staining and histology

We dissected embryos from the uterus at days E8.5–E12.5, fixed the embryos in 4% (v/v) paraformaldehyde (PFA), diluted in phosphate buffered saline (PBS), and stained overnight with X-gal (Promega , Madison, WI). We photodocumented embryos, post-fixed in 4% PFA and then dehydrated, paraffin embedded, sectioned transversely on a Leica microtome at 10μm, and counterstained with Nuclear Fast Red (Sigma-Aldrich , St. Louis, MO), or

hematoxylin and eosin (Sigma-Aldrich , St. Louis, MO) for histologic analysis. Sections were visualized using a Nikon Eclipse E400 or Zeiss light microscope.

Left ventricle measurements

After sectioning and histologic staining as described above, measurements of the left ventricle were made by capturing images of transverse sections of E14.5 hearts from *Shroom3gt/gt* and *Shroom3+/+* littermate control embryos and selecting a matching plane of section which included a 4-chamber view of the heart. All measurements were made in ImageJ. The compact myocardium was measured at the lowest point of the left ventricular wall where it meets the ventricular septum, averaging 10 measurements from each image, and averaging 3 images for each embryo. We compared *Shroom3gt/gt* hearts and *Shroom3+/+* littermate control hearts using the average from each embryo and a Fisher's two-sided t-test for statistical analysis.

Whole mount RNA in situ hybridization (WISH)

Anti-sense digoxigenin-labeled *Shroom3* riboprobes were synthesized with T7 polymerase (Promega, Madison, WI) and DIG-Labeling Mix (Roche, Basel, Switzerland) with a template plasmid[42] kindly provided by Steven Vokes from the University of Texas at Austin. All results are representative images from at least three embryos per embryonic stage.

Immunofluorescence

We performed immunofluorescence on both paraffin sections and cryosections. For paraffin sections, antigen retrieval was performed using Tris-EDTA Buffer (10mM Tris base, 1mM EDTA solution, 0.05% (v/v) Tween 20, pH 9.0) or sodium citrate buffer (10mM Sodium Citrate, 0.05% (v/v) Tween 20, pH 6.0) in a water bath at 100°C for 20–30 minutes. For cryosectioning, we fixed the embryos in 4% PFA overnight, cryoprotected in a sucrose gradient, embedded in Tissue-Tek OCT medium and sectioned on a Leica cryostat at 10μm. Primary and secondary antibodies used are provided (Supplemental Table 1). We capture immunofluorescence images of ISL1, AP-2α, cTnT, and X-gal in *Shroom3+/gt* embryos at E9.5, E10.5, E11.5 and E12.5 using a Nikon Eclipse E400 microscope.

We captured immunofluorescence images of β-catenin in paraffin embedded E10.5 embryos, images of Scribbled (Scrib) and sarcomeric α Actinin (α-actinin) in cryoembedded E11.5 whole embryos and phosphorylated myosin regulatory light chaing (pMLC) and F-actin in cryoembedded E14.5 isolated hearts. We imaged a minimum of three *Shroom3gt/gt* and three *Shroom3+/+* littermate control embryos. We captured images using a Nikon Eclipse E400 fluorescent microscope as well as a Leica SP8 laser-scanning confocal microscope. To measure cardiomyocyte size, roundness and lacunarity, we analyzed a segment of the left ventricular wall adjacent to the ventricular septum in an average of 50 cells from *Shroom3gt/gt* (n=3) and *Shroom3+/+* (n=4) littermate control embryos, utilizing immunofluorescence analysis for cTnT to demarcate cardiomyocytes, followed by Image J to outline and measure cardiomyocyte size and roundness. We analyzed lacunarity utilizing immunofluorescence for F-actin to outline all cells. To quantify lacunarity we utilized a Leica SP8 laser-scanning confocal microscope to capture 1024×1024 images, imaging the lowest point of the left ventricular wall where it meets the ventricular septum. Cells were

segmented using Figi software and cell shape analysis was performed utilizing the Metapmorph plugin to quantify the area between cells, or lacunarity, from $Shroom3^{gt/gt}$ (n=4) and $Shroom3^{+/+}$(n=3) littermate controls. For proliferation and apoptosis analyses we utilized immunofluorescence of caspase 3 or phosphorylated histone H3 (pHH3) as well as cardiac troponin T (cTnT) to identify cardiomyocytes in the left ventricle in matching transverse sections of littermate $Shroom3^{gt/gt}$ and control embryos. We quantified all positive cardiomyocytes (positive for caspase 3 or pHH3 and cTnT) in the entire $1mm^2$ visual field, averaged from 3–4 sections, from $Shroom^{+/+}$ (n=4) and littermate $Shroom3^{gt/gt}$ (n=3) embryos. All counting and analyses were performed blinded. We used the average from each embryo for statistical analysis, comparing $Shroom3^{gt/gt}$ and $Shroom3^{+/+}$ using two-sided t-test for significance.

RT-qPCR

Embryos were harvested at E12.5, a developmental stage of active $Shroom3$ expression coinciding with ventricular chamber morphogenesis and OFT elongation. Whole hearts were harvested for RNA extraction and total RNA was obtained using a mirVana total RNA isolation kit (Thermo-Fisher, Waltham, MA). RNA quality and quantity was assessed by using a NanoDrop One microvolume UV-Vis spectrophotometer (Thermo-Fisher, Waltham, MA). We reverse transcribed RNA using High Capacity RNA to cDNA Reverse Transcription Kit (Thermo-Fisher, Waltham, MA). We utilized Taqman Multiplex Mastermix (Thermo-Fisher, Waltham, MA) and TaqMan probes (Supplemental Table 1). RT-qPCR analysis was performed on a lifecycle Quant Studio 6. $Gapdh$ was used as a control gene to normalize expression data using a comparative CT method. Statistical analysis is described in the figure legend.

Immunoblotting

Whole hearts from embryos were collected at E14.5 and homogenized in RIPA buffer containing a protease/phosphatase inhibitor cocktail (Thermo Fisher, Waltham, MA). Homogenates were centrifuged at $14,000 \times g$ for 15 minutes. We quantified protein using the Pierce™ BCA Protein Assay Kit (Thermo Fisher, Waltham, MA). We utilized 10μg of protein for cytoskeletal proteins, 20μg of protein for PCP proteins and 40μg of protein to detect phosphorylated proteins. We mixed protein lysates with Laemmli buffer (Bio-Rad, Hercules, CA) containing 10% (v/v) β-mercaptoethanol , resolved them on a 4–20% polyacrylamide SDS Novex Wedge Well gel (Invitrogen; Thermo Fisher Scientific, Waltham, MA), transferred to a PVDF membrane and immunodetected target proteins using the chemiluminescent system Clarity™ Western ECL blotting substrate (Bio-Rad, Hercules, CA). GAPDH was utilized as a loading control. Primary and secondary antibodies used are provided (Supplemental Table 1). Blots were visualized using a Bio-Rad Gel Doc system and analyzed in ImageJ.

Co-immunoprecipitation assay (Co-IP)

We utilized a Pierce™ Co-Immunoprecipitation Kit (Thermo-Fisher, Waltham, MA) and performed the Co-IP assay according to the manual. Briefly, we incubated agarose beads with anti-SHROOM3 antibody (ThermoFisher, Waltham, MA), for 2 hours at 4°C. P7 mice hearts were lysed with IP Lysis buffer, precleared with control agarose beads and then

incubated with the anti-SHROOM3 antibody agarose beads overnight at 4°C. We then resolved the proteins on an immunoblot and use an antibody to detect DVL2.

Mouse embryonic fibroblast (MEF) generation, stimulation and immunofluorescence analysis

We harvested MEFs using an established protocol[43], collecting embryos at E12.5–E14.5, mincing embryos, lysing for 1 hour at 37 degrees in 0.25% trypsin (Thermo-Fisher, Waltham, MA), and replating onto 100×17mmNunc cell culture/petri dishes (Thermo-Fisher, Waltham, MA). Cells were split the next day using 0.5% trypsin and every 3–5 days thereafter when confluent. Cells were maintained in DMEM (Thermos-Fisher, Waltham, MA) in 10% Fetal Bovine Serum, (Thermo-Fisher, Waltham, MA.) All assays were performed from passage 2–4. MEF cells underwent PCP pathway stimulation using an established protocol[44] as follows. At passage 2–3, cells were plated to chamber slides. Slides that were confluent on day 3 after splitting were serum starved for 24 hours, after which we generated 3 wounds across the chamber slide using a pipette tip. We then replaced the serum starved media with media supplemented with recombinant 200ng/mL recombinant Wnt5a protein (R&D, Minneapolis, MN). After 24 hours cells were fixed in 4% PFA and immunofluorescence analysis was performed. An average of three images of the wound area were generated using a Nikon Eclipse E400 fluorescent microscope from *Shroom3*[gt/gt] (n=4) and *Shroom3*^{+/+} (n=3) litter matched control embryos. Cells that had moved into the wound area over the previous 24 hours were analyzed. We counted total cells and cells with positive immunofluorescence for activated-phosphorylated MYPT1. Fisher's two-sided t-test was used to compare the average from each embryo MEF line for statistical analysis.

Results

Shroom3 is expressed within the embryonic mouse heart from day E10.5 throughout cardiac development

Shroom3[gt/gt] mice contain a *β-galactosidase* expression cassette inserted between exons 4 and 5 that disrupts efficient RNA splicing, resulting in a complete loss of the SHROOM3 protein and allowing for visualization of *Shroom3* expression via X-gal staining[4]. In order to determine if the expression of the *β-galactosidase* expression cassette truly reflects *Shroom3* mRNA expression, we compared *Shroom3* WISH with whole mount X-gal staining in *Shroom3*[+/gt] mouse embryos at E9.5 (Fig. 1).

Results show that at E9.5 *Shroom3* message is detectable within the frontonasal process of the head and lateral and splanchnic mesoderm just dorsal to the cardiac OFT (Fig. 1 A and C). *Shroom3* expression within the heart itself is undetectable. X-gal staining in *Shroom3*[+/gt] E9.5 embryos recapitulate expression domains observed by WISH (Fig. 1 B and D). In E10.5 and E12.5 *Shroom3*[+/gt] embryos, X-gal staining within the heart is detectable within the right atria (ra), left atria (la), right ventricular (rv) and left ventricular (lv) myocardium (Fig. 1 E–H, K, and L).

Sections of X-gal staining in *Shroom3*[+/gt] E10.5 embryos revealed expression within the aortic sac (as) as well as the OFT myocardium (Fig. 1 I, Fig. 1 J, arrow). E10.5 sections of

X-gal staining of *Shroom3*[+/gt] embryos also reveal robust expression with the rv and lv myocardium as well as strong staining in cardiomyocytes within the forming interventricular septum (ivs) (Fig. 1 K and L). X-gal staining within the atrioventricular cushion (avc) is not detected in *Shroom3*[+/gt] embryos.

We detected *Shroom3* expression in the heart throughout embryonic development and into the neonatal and adult period, with X-gal staining within all four cardiac chambers at P7 (Supplemental Fig. 1A), P21 (Supplemental Fig. 1B), 3 months (Supplemental Fig. 1C) and 9 months (Supplemental Fig. 1D). We confirmed *Shroom3* expression in four cardiac chambers during the neonatal and adult period with gene expression analysis by qRT-PCR in *Shroom3*^{+/+} mice in the rv, lv, ra, la and ivs at P45 and 1 year (Supplemental Fig. 1E).

Shroom3 is expressed in cardiomyocytes, cardiac neural crest cells and second heart field cells

The expression of *Shroom3* within the aortic sac suggests cardiac neural crest cell expression of *Shroom3*. To determine this, we directly compared E9.5 X-gal stained sections of *Shroom3*[+/gt] embryos with sections immunostained with the cardiac neural crest marker AP-2α (Fig. 2). Results show overlap of *Shroom3* X-gal staining in the aortic sac and immunofluorescence for AP-2α in E9.5 *Shroom3*[+/gt] embryos (Fig. 2 A and B, black and white arrowheads respectively).

Shroom3[+/gt] embryos also demonstrate X-gal staining within the OFT myocardium, suggesting *Shroom3* second heart field expression. To determine this, we directly compared E10.5 X-gal stained sections of E10.5 *Shroom3*[+/gt] embryos with serial sections immunostained with the second heart field marker *Islet1* (ISL1) (Fig. 2). Results show overlap of *Shroom3* X-gal staining within the OFT myocardium and immunofluorescence of ISL1 within E10.5 *Shroom3*[+/gt] embryos (Fig. 2 C and D, black and white arrowheads, respectively).

Given the robust X-gal staining observed within the rv, lv, and ivs, we confirmed *Shroom3* expression within cardiomyocytes. E12.5 *Shroom3*[+/gt] embryo serial sections demonstrate overlapping *Shroom3* X-gal staining (Fig. 3 A and B) and immunofluorescence for cTnT (Fig. 3 C and D). At E11.5, *Shroom3*[+/gt] embryo cryosections demonstrate colocalization of immunofluorescence for X-gal and immunofluorescence for cTnT (Fig. 3 E–G).

Shroom3[gt/gt] mice exhibit cardiac defects including ventricular septal defects, double outlet right ventricle and left ventricular noncompaction

We next assessed cardiac morphology in hematoxylin and eosin stained transverse sections of *Shroom3*^{+/+} and *Shroom3*[gt/gt] littermate embryo hearts at E14.5, when cardiac septation is complete. When compared to controls (Fig. 4 A and D) *Shroom3*[gt/gt] embryos display frequent but not fully penetrant cardiac defects (Fig. 4 B, C, E and F). The spectrum of defects observed are consistent with those observed in other PCP knockout mice including membranous VSD (Fig. 4 B, asterisk), in which the ventricular septum fails to fully separate the rv and lv circulation. S*hroom3*[gt/gt] mutant hearts also exhibit muscular VSDs (Fig. 4 C, arrowhead). In contrast to *Shroom3*^{+/+} littermate controls, in which the aorta connects directly with the lv (Fig. 4 D), 19% of *Shroom3*[gt/gt] hearts exhibit DORV, in which both the

aorta and pulmonary artery directly connect with the rv (Fig. 4 E, asterisk). Interestingly, we also observed one *Shroom3*[gt/gt] heart with double inlet left ventricle, in which both the tricuspid valve (tv) and mitral valve (mv) directly connect with the lv (Fig. 4 F). A summary of observed cardiac phenotypes is presented (Fig. 4 G). *Shroom3*[gt/gt] mice also exhibit ventricular thinning (Fig. 4 H), with LV walls 36% thinner than wild type littermate controls.

SHROOM3 interacts with key PCP signaling component DVL2 in the heart and *Shroom3*[gt/gt] mice have disrupted terminal PCP components in the heart

Given that SHROOM3 interacts with PCP components ROCK1[16] and DVL2[17], drives cellular planar cell polarity[18], and results in CHD characteristic of PCP disruption in *Shroom3*[gt/gt] mice (Fig. 4), we sought to investigate potential alterations in PCP due to SHROOM3 loss during cardiac development. The PCP pathway is activated by the WNT-ligands WNT5a and WNT11 through one of 3 transmembrane receptors: Frizzled (FZD), Cadherin EGF LAG seven-pass G-type receptor (CELSR), or Vangl-like (VANGL). Receptor signaling then activates at least 3 cytoplasmic protein families: DVL, SCRIB, and Prickle (PK). The final tier of PCP signaling includes the Actomyosin cytoskeleton effectors DAAM1, RAS homolog gene family, member A (RHOA), JNK and ROCK1[45] (Fig. 5 A). These components, through differential positioning within a cell, establish cellular polarity and directionality. The signal propagates to adjacent cells, polarizing both epithelial and mesenchymal tissues[45].

DVL2 is the key cytoplasmic component of the planar cell polarity pathway making up 95% of DISHEVELED proteins. It has been demonstrated that SHROOM3 and DVL2 colocalize and form a physical complex within cells of the neural tube[17]. To investigate interaction within the heart, we utilized a Co-IP assay in neonatal mouse heart lystate, demonstrating that DVL2 binds to SHROOM3 (Fig. 5 B).

To determine if *Shroom3* expression is altered under conditions of disrupted PCP signaling, we analyzed *Shroom3* gene expression using a well validated model of PCP disruption, *Dvl2* conditional mice. We generated *Dvl2*^{−/−} mice by crossing conditional *Dvl2*[flox/flox] males with *Sox2-Cre* females. *Sox2-Cre* is expressed within the female germ line producing a heritable knockout allele[46]. We quantified *Shroom3* expression after PCP disruption using gene expression analysis. Gene expression analysis from whole hearts isolated from *Dvl2*^{−/−}, *Dvl2*^{+/−} and *Dvl2*^{+/+} littermate control embryos at E12.5, revealed a 60% decrease in *Shroom3* expression in *Dvl2*^{−/−} embryonic hearts (Fig. 5 C).

We next sought to investigate the temporal and spatial downregulation of *Shroom3* in the embryonic heart. To do this we analyzed *Shroom3* expression in *Dvl2*^{−/−} and *Dvl2*^{+/+} littermate control embryos, again utilizing whole mount X-gal staining in *Shroom3*[+/gt] mouse embryos as well as *Shroom3* WISH to detect *Shroom3* expression. When compared to *Dvl2*^{+/+} littermate control embryos (Fig. 5 D, F and H), *Dvl2*^{−/−} embryos have a global decrease in *Shroom3* expression throughout the heart, beginning at the start of Shroom3 expression at E10.5 (Fig. 5E), and persisting through OFT formation and ventricular maturation at E11.5 (Fig. 5G) and E12.5 (Fig. 5 I). Reduced *Shroom3* expression was revealed by both X-gal staining in *Shroom3*[+/gt];*Dvl2*^{−/−} E10.5 embryos (Fig. 5 E), as well as *Shroom3* WISH in E11.5 *Dvl2*^{−/−} (Fig. 5 G) and E12.5 *Dvl2*^{−/−} embryos (Fig. 5 I). X-gal

staining in *Shroom3*[+/gt] embryos again recapitulates expression domains observed by WISH. Robust downregulation of *Shroom*3 after disruption of the key cytoplasmic PCP component within the heart demonstrates that *Shroom3* expression is modulated by alterations in PCP signaling and suggests that SHROOM3 sits downstream of DVL2 in the PCP pathway during cardiac development.

There is strong genetic interaction between PCP components during cardiac development: for example *Vangl2* heterozygous mice are phenotypically normal but compound heterozygous mice with *Vangl2* and another PCP component have defects including CHD 32,33,35. To explore a genetic interaction between SHROOM3 and DVL2, we crossed *Shroom3*[+/gt] and *Dvl2*^{+/−} mice, which are each phenotypically normal, to generate litters of compound heterozygous *Shroom3*[+/gt];*Dvl2*^{+/−} mice, and harvested embryos at day E14.5, just after closure of the ventricular septum. We demonstrate that singly heterozygous *Shroom3*[+/gt];*Dvl2*^{+/+} (Fig. 5 J and K) and *Shroom3*^{+/+};*Dvl2*[+/−](Fig. 5 L and M) littermates were normal, consistent with the literature[4,25], however we observed PCP associated cardiac defects, including membranous VSD (Fig. 5 O) and DORV (Fig. 5 N), in a compound heterozygous *Shroom3*[+/gt];*Dvl2*^{+/−} embryo. There was also a trend towards decreased survival in the SHROOM3 and DVL2 compound heterozygous embryos, though not statistically significant, limited by small sample size (Supplemental Table 2.) To further explore genetic interaction between SHROOM3 and DVL2 we generated double knockout mice by crossing *Shroom3*[+/gt];*Dvl2*^{+/−} mice to *Shroom3*[+/gt];*Dvl2*^{−/−} mice, and again harvested embryos at day E14.5. Of note, phenotypic abnormalities due to DVL2 loss demonstrate a gender bias, with previous studies showing greater effect on males[25], and our findings confirmed this as we recovered no male *Shroom3*[gt/gt];*Dvl2*^{+/−} or *Shroom3*[gt/gt];*Dvl2*^{−/−} mice (0 observed, versus 4.75 expected, p=0.0385). PCP associated cardiac defects in a compound heterozygous *Shroom3*^{+/+};*Dvl2*^{+/−} embryo suggests SHROOM3 and PCP's key cytoplasmic component DVL2 interact genetically during cardiac development.

Given the evidence for genetic interaction between SHROOM3 and a key PCP cytoplasmic component, we sought to analyze the effect of *Shroom3* disruption on the activation of PCP pathway terminal components. A downstream effect of PCP signaling results in ROCK1 phosphorylating MLC as well as myosin light chain phosphatase (MYPT1), which leads to increased phosphorylated -and activated- MLC. We utilized an established assay of PCP activation: stimulating cells with PCP ligand WNT5a and assaying PCP terminal component phosphorylated MYPT1. We generated MEFs from *Shroom3*^{+/+} and *Shroom3*[gt/gt] littermates, stimulated the MEFs with WNT5a and performed immunofluorescence analysis of phosphorylated MYPT1 (Fig. 5 P–U). We demonstrate that compared with *Shroom3*^{+/+} MEFs (Fig. 5 P, Q and R), *Shroom3*[gt/gt] MEFs (Fig. 5 S, T and R) have significantly reduced activated MYPT1 (Fig. 5 V).

Given that *Shroom3* alteration disrupted PCP signaling pathway activation in cultured cells, we sought to determine the effect of *Shroom3* loss-of-function on transcriptional regulation of terminal PCP signaling components within the heart. We performed gene expression analysis of whole hearts from E12.5 *Shroom3*^{+/+} control and littermate *Shroom3*[gt/gt] mutants (Fig. 5 W). Results show that *Shroom3*[gt/gt] hearts have evidence of PCP gene expression

dysregulation, with significant decreases in *Daam1, JNK*, and *RhoA*, observed. Although there is a trend in *Rac1* decrease, the genes *Rac1* and *Rock1* are not significantly downregulated in *Shroom3^gt/gt^* hearts (Fig. 5 W). These findings suggest that loss of *Shroom3* expression leads to significant changes in the gene expression within the PCP pathway, revealing a possible feedback mechanism affecting multiple genes within this signaling pathway.

To demonstrate the effect of *Shroom3* loss-of-function on PCP proteins within the heart, we performed immunoblot analysis on E12.5 *Shroom3^+/+^* and *Shroom3^gt/gt^* littermate whole heart lysates (Fig. 5 X). We quantified the activation of PCP by measuring the activated, phosphorylated, versus inactive, unphosphorylated PCP central component DVL2 as well as terminal components MYPT1 and MLC within the heart. *Shroom3^gt/gt^* hearts exhibit observable reductions in the activated form of multiple PCP proteins including: phosphorylated MYPT1, phosphorylated MLC (pMLC), and phosphorylated DVL2 (pDVL2)(Fig. 5 X).

*Shroom3^gt/gt^* mouse hearts exhibit cardiomyocyte disorganization and loss of polarity within the outflow tract and ventricle

Given *Shroom3^gt/gt^* cardiac defects (Fig. 4), and altered PCP signaling (Fig. 5), we sought to demonstrate the effect on cellular morphology, tissue polarization and organization in the affected progenitor tissues throughout cardiac development, and the progression of the phenotype at multiple stages. Within the developing heart, PCP drives OFT elongation[27] and studies have demonstrated loss of PCP components *Wnt5a, Wnt11, Frizzled 1-2, Prickle1, Scrib1, Dvl1-3*, and *Vangl2*, causes OFT disruption leading to cardiac defects identical to those we observed in *Shroom3^gt/gt^* mice[25,26,29–36]. Therefore we assayed OFT wall structure and cellular polarity at E10.5 during active OFT elongation and the start of robust *Shroom3* expression (Fig. 6 A–D). We assessed cellular polarity within the OFT using immunofluorescence analysis of an established adherens-junction component, β-catenin, in the OFT of E10.5 *Shroom3^+/+^* (Fig. 6 A and B) and littermate *Shroom3^gt/gt^* embryos (Fig.6 C and D). In the *Shroom3^+/+^* OFT membrane, cells are organized and aligned, with β-catenin localized to adherens junctions (Fig. 6 B, arrowheads). The *Shroom3^gt/gt^* OFT membrane cells are disorganized with loss of β-catenin localization at the adherens junctions (Fig. 6 D, arrowheads).

At later stages of cardiac development, PCP drives ventricular cardiomyocyte maturation including polarization, elongation, and ventricular thickening, and mice null for *Wnt11, Scrib, Daam1* or *Vangl2* have ventricular thinning similar to the *Shroom3^gt/gt^* mice[30,32,37,38]. In these other PCP models, ventricular thinning is associated with cardiomyocyte disorganization, spherical shape, and disrupted actomyosin. Therefore we analyzed left ventricular cardiomyocyte polarity and organization, starting at E11.5, during active ventricular morphogenesis (Fig. 6 E–H). We performed immunofluorescence analysis of polarity using an established basolateral membrane marker and PCP component SCRIB and a cardiomyocyte marker sarcomeric α-actinin (α-actinin) in the ventricular wall of E11.5 *Shroom3^+/+^* (Fig. 6 E and F) and littermate *Shroom3^gt/gt^* embryos (Fig.6 G and H). We demonstrate the ventricular wall of *Shroom3^+/+^* mice is compact and organized with well

aligned cells and SCRIB localized at the basolateral membrane of the ventricular epicardium (Fig. 6 F, arrowhead). On the contrary, *Shroom3*$^{gt/gt}$ ventricular wall cardiomyocytes are disorganized and less-compact with more space between cells, and without evident SCRIB at the basolateral membrane of the ventricular epicardium (Fig.6. H, arrowhead) (though still evident in the atria basolateral membrane) (Fig. 6. G, arrow). This cardiomyocyte disorganization and disrupted polarity is consistent with PCP disruption which may lead to LVNC in the developing ventricle.

PCP drives developmental processes by altering the Actomyosin cytoskeleton, impacting cellular shape and movement. Mutants for PCP ligand Wnt5a and PCP cytoplasmic components Dvl1/2 display aberrant cell packing due to defective Actomyosin polymerization and filopodia formation within the heart[27]. In *Xenopus*, PCP signaling drives Actomyosin organization in the cardiac OFT; and in both zebrafish and mice, PCP drives ventricular wall cardiomyocyte maturation and organization. *Shroom3*$^{gt/gt}$ mice exhibit Actomyosin cytoskeletal disruption within the neural tube, gut, kidney, and lens of the eye[6,9–12,14]. Therefore, we investigated cytoskeletal disruption in the hearts of *Shroom3*$^{gt/gt}$ mutants by observing cytoskeletal organization of F-actin and pMLC immunofluorescence analysis of E14.5 *Shroom3*$^{+/+}$ and littermate *Shroom3*$^{gt/gt}$ hearts (Fig. 6 I–N). Ventricular septum closure occurs, and ventricular morphogenesis is active, at E14.5, making it an ideal timepoint to assess PCP defects including septal defects and ventricular noncompaction. *Shroom3*$^{gt/gt}$ hearts exhibit histologic changes within the OFT and lv that are characteristic of PCP disruption. In the *Shroom3*$^{+/+}$ ventricular septum, cells exhibit indicators of cellular movement including visible lamellipodia and filopodia (Fig. 6 J, arrowheads). In contrast, *Shroom3*$^{gt/gt}$ septal cardiomyocytes appear rounded, lacking lamellipodia and filopodia, and fail to achieve septal closure with an evident membranous VSD (Fig. 6 M, asterisk).

PCP is implicated in ventricular maturation and myocardial polarization, and multiple PCP knockout mouse models exhibit ventricular thinning with spherical, immature, and disorganized cardiomyocytes [30,32,37,38]. In *Shroom3*$^{+/+}$ mouse lv walls the majority of cardiomyocytes appear mature and elongated and show organized sarcomeres (Fig. 6 K, arrowheads), whereas *Shroom3*$^{gt/gt}$ littermate hearts contain lv wall cardiomyocytes that appear rounded and disorganized (Fig. 6 N, arrowheads).

We next quantified this cardiomyocyte phenotype utilizing immunofluorescence analysis of cardiomyocyte marker cTnT in E14.5 *Shroom3*$^{+/+}$ and littermate *Shroom3*$^{gt/gt}$ hearts (Fig. 6 O–Q.) Given the thinned left ventricle wall (Fig. 3), we began measuring cardiomyocyte size, as total area, and found no difference (Gig 6 O.) During maturation cardiomyocytes lose sphericity and elongate, therefore, to assess maturity we measured cardiomyocyte roundness, demonstrating that compared to *Shroom3*$^{+/+}$ littermate controls, *Shroom3*$^{gt/gt}$ embryo cardiomyocytes are significantly more round (Fig.6. P). To assay disorganization and compaction, we measured lacunarity, or the average space between cells, and found that compared to *Shroom3*$^{+/+}$ littermate controls, *Shroom3*$^{gt/gt}$ embryo cardiomyocytes are also significantly less compact and more disorganized (Fig.6. Q).

Shroom3^gt/gt mouse hearts exhibit increased cardiomyocyte proliferation

In addition to OFT defects, mouse models with disrupted PCP components *Wnt11, Vangl, Scrib, and Daam* have ventricular pathology phenocopying *Shroom3* loss, with immature, spherical, cardiomyocytes, and a thinned and underdeveloped left ventricle resembling LVNC. The left ventricle phenotype in LVNC has been attributed to dysregulated cell cycle, with a study in PCP component *Daam1/2*[47] describing decreased ventricular wall cardiomyocyte maturation and increased cardiomyocyte proliferation. To explore whether ventricular phenotype in *Shroom3* mice is due to cardiomyocyte proliferation or apoptosis we performed immunofluorescence analysis of cell proliferation marker pHH3 as well as cellular apoptosis marker activated-caspase 3 within the lv wall of *Shroom*^+/+ mice and litter matched *Shroom3*^gt/gt embryos at E9.5 and at E14.5. Compared with *Shroom3*^+/+ littermates (Fig. 7 A and C), *Shroom3*^gt/gt embryos have observably increased cardiomyocyte proliferation within the left ventricle at both E9.5 (Fig. 7 B), and at E14.5 (Fig. 7 D). We quantified this increased proliferation in E14.5 left ventricular wall cardiomyocytes (Fig. 7 E).

Some LVNC mouse models have increased cardiomyocyte proliferation localized to the trabecular cardiomyocytes[48]. Therefore we analyzed sections of the left ventricle and found *Shroom3*^gt/gt mice have similarly increased proliferation localized to the ventricular trabeculae (Fig. H), whereas cardiomyocyte proliferation within the lv wall (Fig. F) and septum (Fig. G) are normal. We also observed a congruent trend towards decreased apoptosis *Shroom3*^gt/gt embryo lv, though not significant (Supplemental Fig. 2.) The increased ventricular proliferation phenocopying other PCP loss-of-function models[47] is consistent with our proposed mechanism of action of SHROOM3.

Discussion

The data in this study are the first to demonstrate that *Shroom3* loss-of-function results in cardiac defects. Additionally, we describe a likely mechanism, highlighting SHROOM3's novel role during cardiac development, as an actomyosin effector downstream of PCP signaling. Though unexplored in cardiac development, previous studies have demonstrated SHROOM3's role in neural tube, gut, lens and kidney development[6,9–12,14], attributed to SHROOM3 driven actomyosin contractility during developmental processes, including apical epithelial constriction[14] and planar polarized convergent extension[18]. SHROOM3 regulates neuroepithelial planar remodeling[16], and functions downstream of the PCP signaling pathway during neural tube development[17], physically interacting with multiple PCP components, including key cytoplasmic component DVL2 in the neural tube. We demonstrate here that SHROOM3 and DVL2 also physically interact in the heart (Fig. 5 B) and interact genetically during cardiac development (Fig. 5 J–O). *Shroom3*^gt/gt mice exhibit OFT phenotypes similar to those observed in loss-of-function models of the PCP components: *Wnt5a, Wnt11, Frizzled 1-2, Prickle1, Scrib1, Dvl1-3*, and *Vangl2*[25,26,29–36,49]. Consistent with these other PCP loss-of-function models, we show that *Shroom3*^gt/gt mice have disorganization and loss of polarity within the OFT (Fig. 6 A–D) and evidence of cellular movement defects, including reduced lamellipodia and filopodia within the OFT cushion (Fig. 6 J and M). These data further support the importance of cell polarity to organ

morphogenesis, likely through the PCP dependent process of convergent extension. We previously identified a *SHROOM3* variant in a patient with a PCP-related CHD phenotype[3] and human *SHROOM3* variants are implicated in additional phenotypes associated with PCP disruption, including neural tube defects and kidney disease[5–8]. These findings along with the *Shroom3^(gt/gt)* mouse phenotype mechanistically point to PCP defects as causative of CHD in mice and likely in humans.

Shroom3^(gt/gt) mice have ventricular thinning along with disorganization and loss of polarity within the ventricular wall cardiomyocytes (Fig. 6 E–N) and epicardium (Fig. 6 E–H). Although the majority of the aforementioned PCP mutations exhibit OFT phenotypes, *Daam1, Scrib, Vangl2* and *Wnt11* loss-of-function mice exhibit similar ventricular wall phenotypes, consistent with LVNC[30,32,37,38]. The LVNC phenotype in PCP has been attributed to dysregulated cell cycle, and a recent study in *Daam1/2*[47] similarly describes left ventricular wall increased cardiomyocyte proliferation. Other LVNC models, including FKB12 loss of function mouse[48], have increased left ventricular cardiomyocyte proliferation localized to the trabeculae. *Shroom3^(gt/gt)* mice have similarly increased cardiomyocyte proliferation localized to trabeculae (Fig. 7). Left ventricular thinning due to PCP disruption is implicated in LVNC cardiomyopathy in humans[50], and may be an additional important clinical implication of *SHROOM3* loss in humans.

Shroom3 has an established role as an Actomyosin effector. Recent studies indicate the importance of PCP's terminal Actomyosin tissue effectors, including DAAM1 and RAC1, during cardiac development[28,38,39] and in CHD. We demonstrate *Shroom3^(gt/gt)* embryo hearts have transcriptional downregulation of PCP terminal effectors (Fig. 5 W) as well as decreased activated proteins (Fig. 5 X). We found no gene expression changes in upstream components including PCP pathway ligands *Wnt5a* or *Wnt11*, or transmembrane receptors *Fzd, Celsr* or *Vangl* (data not shown). We do show that key PCP cytoplasmic component DVL2 interacts with SHROOM3 during cardiac development (Fig. 5 B). These data place SHROOM3 within the PCP pathway downstream of DVL2, among these crucial terminal Actomyosin effectors (Fig. 8). Given that WNT5a sits at the top of PCP pathway and SHROOM3 sits at the terminal effector end of PCP signaling, the similarities in observed phenotypes may demonstrate that SHROOM3 function is vital to carry out PCP signaling during cardiac development.

We observe that *Shroom3^(gt/gt)* mice demonstrate partial penetrance of cardiovascular defects, including ventricular thinning, membranous VSDs, DORV and an example of DILV (Fig. 4 G). *Shroom3^(gt/gt)* mice have previously been shown to have fully penetrant neural tube defects as well as partially penetrant lens, gut and kidney defects. Previously described cardiac defects within PCP mutants exhibit partial to full penetrance[25,26,28–39,49,51]. Partial penetrance of cardiac defects in *Shroom3^(gt/gt)* mice could reflect that other terminal PCP components, (or possibly other SHROOM proteins) provide a compensatory mechanism for PCP driven actomyosin rearrangements in the absence of SHROOM3.

Conclusion

This study represents the first description of SHROOM3 loss-of-function leading to cardiac defects and provides a mechanism, demonstrating disrupted PCP pathway activation and cytoskeleton rearrangements, affecting cardiomyocyte polarity, organization and proliferation. These data describe a new role for SHROOM3 during cardiac development and strengthen the evidence for SHROOM3's role downstream of the PCP pathway as a terminal actomyosin effector. Identifying a novel CHD gene and exploring its role in a fundamental signaling pathway is important for our understanding of cardiac development.

Supplementary Material

Refer to Web version on PubMed Central for supplementary material.

Acknowledgments

List of abbreviations

ao	aorta
as	aortic sac
DILV	double inlet left ventricle
DORV	double outlet right ventricle
ht	heart
ivs	intraventricular septum
la	left atrium
lv	left ventricle
oft	outflow tract
mv	mitral valve
pa	pulmonary artery
rv	right ventricle
ra	right atrium

tv	tricuspid valve

References

1. Mozaffarian D, Benjamin EJ, Go AS, et al. Executive Summary: Heart Disease and Stroke Statistics--2016 Update: A Report From the American Heart Association. Circulation. 2016;133(4):447–454. [PubMed: 26811276]

2. Ransom J, Srivastava D. The genetics of cardiac birth defects. Paper presented at: Seminars in cell & developmental biology 2007.

3. Tariq M, Belmont JW, Lalani S, Smolarek T, Ware SM. SHROOM3 is a novel candidate for heterotaxy identified by whole exome sequencing. Genome biology. 2011;12(9):R91. [PubMed: 21936905]

4. Hildebrand JD, Soriano P. Shroom, a PDZ domain–containing actin-binding protein, is required for neural tube morphogenesis in mice. Cell. 1999;99(5):485–497. [PubMed: 10589677]

5. Menon MC, Chuang PY, Li Z, et al. Intronic locus determines SHROOM3 expression and potentiates renal allograft fibrosis. The Journal of clinical investigation. 2015;125(1):208–221. [PubMed: 25437874]

6. Khalili H, Sull A, Sarin S, et al. Developmental origins for kidney disease due to Shroom3 deficiency. Journal of the American Society of Nephrology. 2016:ASN. 2015060621.

7. Yeo NC, O'Meara CC, Bonomo JA, et al. Shroom3 contributes to the maintenance of the glomerular filtration barrier integrity. Genome research. 2015;25(1):57–65. [PubMed: 25273069]

8. Lemay P, Guyot M-C, Tremblay É, et al. Loss-of-function de novo mutations play an important role in severe human neural tube defects. Journal of medical genetics. 2015;52(7):493–497. [PubMed: 25805808]

9. Plageman TF, Chung M-I, Lou M, et al. Pax6-dependent Shroom3 expression regulates apical constriction during lens placode invagination. Development. 2010;137(3):405–415. [PubMed: 20081189]

10. Chung M-I, Nascone-Yoder NM, Grover SA, Drysdale TA, Wallingford JB. Direct activation of Shroom3 transcription by Pitx proteins drives epithelial morphogenesis in the developing gut. Development. 2010;137(8):1339–1349. [PubMed: 20332151]

11. Plageman TF, Zacharias AL, Gage PJ, Lang RA. Shroom3 and a Pitx2-N-cadherin pathway function cooperatively to generate asymmetric cell shape changes during gut morphogenesis. Developmental biology. 2011;357(1):227–234. [PubMed: 21726547]

12. Lang RA, Herman K, Reynolds AB, Hildebrand JD, Plageman TF. p120-catenin-dependent junctional recruitment of Shroom3 is required for apical constriction during lens pit morphogenesis. Development. 2014;141(16):3177–3187. [PubMed: 25038041]

13. Plageman TF, Chauhan BK, Yang C, et al. A Trio-RhoA-Shroom3 pathway is required for apical constriction and epithelial invagination. Development. 2011;138(23):5177–5188. [PubMed: 22031541]

14. Haigo SL, Hildebrand JD, Harland RM, Wallingford JB. Shroom induces apical constriction and is required for hingepoint formation during neural tube closure. Current biology. 2003;13(24):2125–2137. [PubMed: 14680628]

15. Hildebrand JD. Shroom regulates epithelial cell shape via the apical positioning of an actomyosin network. Journal of cell science. 2005;118(22):5191–5203. [PubMed: 16249236]

16. Nishimura T, Takeichi M. Shroom3-mediated recruitment of Rho kinases to the apical cell junctions regulates epithelial and neuroepithelial planar remodeling. Development. 2008;135(8):1493–1502. [PubMed: 18339671]

17. McGreevy EM, Vijayraghavan D, Davidson LA, Hildebrand JD. Shroom3 functions downstream of planar cell polarity to regulate myosin II distribution and cellular organization during neural tube closure. Biology open. 2015;4(2):186–196. [PubMed: 25596276]

18. Simões SdM, Mainieri A, Zallen JA. Rho GTPase and Shroom direct planar polarized actomyosin contractility during convergent extension. Journal of Cell Biology. 2014;204(4):575–589.

19. Wu G, Ge J, Huang X, Hua Y, Mu D. Planar cell polarity signaling pathway in congenital heart diseases. BioMed Research International. 2011;2011.

20. Henderson DJ, Chaudhry B. Getting to the heart of planar cell polarity signaling. Birth Defects Research Part A: Clinical and Molecular Teratology. 2011;91(6):460–467. [PubMed: 21538810]

21. Axelrod JD. Progress and challenges in understanding planar cell polarity signaling. Paper presented at: Seminars in cell & developmental biology 2009.

22. Carmona-Fontaine C, Matthews HK, Kuriyama S, et al. Contact inhibition of locomotion in vivo controls neural crest directional migration. Nature. 2008;456(7224):957. [PubMed: 19078960]

23. De Calisto J, Araya C, Marchant L, Riaz CF, Mayor R. Essential role of non-canonical Wnt signalling in neural crest migration. Development. 2005;132(11):2587–2597. [PubMed: 15857909]

24. Matthews HK, Marchant L, Carmona-Fontaine C, et al. Directional migration of neural crest cells in vivo is regulated by Syndecan-4/Rac1 and non-canonical Wnt signaling/RhoA. Development. 2008;135(10):1771–1780. [PubMed: 18403410]

25. Hamblet NS, Lijam N, Ruiz-Lozano P, et al. Dishevelled 2 is essential for cardiac outflow tract development, somite segmentation and neural tube closure. Development. 2002;129(24):5827–5838. [PubMed: 12421720]

26. Schleiffarth JR, Person AD, Martinsen BJ, et al. Wnt5a is required for cardiac outflow tract septation in mice. Pediatric research. 2007;61(4):386. [PubMed: 17515859]

27. Sinha T, Wang B, Evans S, Wynshaw-Boris A, Wang J. Disheveled mediated planar cell polarity signaling is required in the second heart field lineage for outflow tract morphogenesis. Developmental biology. 2012;370(1):135–144. [PubMed: 22841628]

28. Leung C, Liu Y, Lu X, Kim M, Drysdale TA, Feng Q. Rac1 signaling is required for anterior second heart field cellular organization and cardiac outflow tract development. Journal of the American Heart Association. 2015;5(1):e002508. [PubMed: 26722124]

29. Phillips HM, Murdoch JN, Chaudhry B, Copp AJ, Henderson DJ. Vangl2 acts via RhoA signaling to regulate polarized cell movements during development of the proximal outflow tract. Circulation research. 2005;96(3):292–299. [PubMed: 15637299]

30. Nagy II, Railo A, Rapila R, et al. Wnt-11 signalling controls ventricular myocardium development by patterning N-cadherin and β-catenin expression. Cardiovascular research. 2009;85(1):100–109.

31. Henderson DJ, Conway SJ, Greene ND, et al. Cardiovascular defects associated with abnormalities in midline development in the Loop-tail mouse mutant. Circulation Research. 2001;89(1):6–12. [PubMed: 11440971]

32. Phillips HM, Rhee HJ, Murdoch JN, et al. Disruption of planar cell polarity signaling results in congenital heart defects and cardiomyopathy attributable to early cardiomyocyte disorganization. Circulation research. 2007;101(2):137–145. [PubMed: 17556662]

33. Etheridge SL, Ray S, Li S, et al. Murine dishevelled 3 functions in redundant pathways with dishevelled 1 and 2 in normal cardiac outflow tract, cochlea, and neural tube development. PLoS genetics. 2008;4(11):e1000259. [PubMed: 19008950]

34. Zhou W, Lin L, Majumdar A, et al. Modulation of morphogenesis by noncanonical Wnt signaling requires ATF/CREB family–mediated transcriptional activation of TGFβ2. Nature genetics. 2007;39(10):1225. [PubMed: 17767158]

35. Yu H, Smallwood PM, Wang Y, Vidaltamayo R, Reed R, Nathans J. Frizzled 1 and frizzled 2 genes function in palate, ventricular septum and neural tube closure: general implications for tissue fusion processes. Development. 2010;137(21):3707–3717. [PubMed: 20940229]

36. Paudyal A, Damrau C, Patterson VL, et al. The novel mouse mutant, chuzhoi, has disruption of Ptk7 protein and exhibits defects in neural tube, heart and lung development and abnormal planar cell polarity in the ear. BMC developmental biology. 2010;10(1):87. [PubMed: 20704721]

37. Phillips HM, Hildreth V, Peat JD, et al. Non–cell-autonomous roles for the planar cell polarity gene Vangl2 in development of the coronary circulation. Circulation research. 2008;102(5):615–623. [PubMed: 18174466]

38. Li D, Hallett MA, Zhu W, et al. Dishevelled-associated activator of morphogenesis 1 (Daam1) is required for heart morphogenesis. Development. 2011;138(2):303–315. [PubMed: 21177343]

39. Leung C, Lu X, Liu M, Feng Q. Rac1 signaling is critical to cardiomyocyte polarity and embryonic heart development. Journal of the American Heart Association. 2014;3(5):e001271. [PubMed: 25315346]

40. Merks AM, Swinarski M, Meyer AM, et al. Planar cell polarity signalling coordinates heart tube remodelling through tissue-scale polarisation of actomyosin activity. Nature communications. 2018;9(1):2161.

41. Ohata S, Nakatani J, Herranz-Pérez V, et al. Loss of Dishevelleds disrupts planar polarity in ependymal motile cilia and results in hydrocephalus. Neuron. 2014;83(3):558–571. [PubMed: 25043421]

42. Lewandowski JP, Du F, Zhang S, et al. Spatiotemporal regulation of GLI target genes in the mammalian limb bud. Developmental biology. 2015;406(1):92–103. [PubMed: 26238476]

43. Qiu L-Q, Lai WS, Stumpo DJ, Blackshear PJ. Mouse embryonic fibroblast cell culture and stimulation. Bio-protocol. 2016;6(13).

44. Liu PY, Liao JK. A method for measuring Rho kinase activity in tissues and cells. Methods in enzymology. 2008;439:181–189. [PubMed: 18374165]

45. Simons M, Mlodzik M. Planar cell polarity signaling: from fly development to human disease. Annual review of genetics. 2008;42:517–540.

46. https://www.jax.org/strain/024637.https://www.jax.org/strain/024637.

47. Ajima R, Bisson JA, Helt J-C, et al. DAAM1 and DAAM2 are co-required for myocardial maturation and sarcomere assembly. Developmental biology. 2015;408(1):126–139. [PubMed: 26526197]

48. Chen H, Zhang W, Sun X, et al. Fkbp1a controls ventricular myocardium trabeculation and compaction by regulating endocardial Notch1 activity. Development. 2013;140(9):1946–1957. [PubMed: 23571217]

49. Curtin JA, Quint E, Tsipouri V, et al. Mutation of Celsr1 disrupts planar polarity of inner ear hair cells and causes severe neural tube defects in the mouse. Current Biology. 2003;13(13):1129–1133. [PubMed: 12842012]

50. Zhang W, Chen H, Qu X, Chang CP, Shou W. Molecular mechanism of ventricular trabeculation/compaction and the pathogenesis of the left ventricular noncompaction cardiomyopathy (LVNC). Paper presented at: American Journal of Medical Genetics Part C: Seminars in Medical Genetics 2013.

51. Murdoch JN, Henderson DJ, Doudney K, et al. Disruption of scribble (Scrb1) causes severe neural tube defects in the circletail mouse. Human molecular genetics. 2003;12(2):87–98. [PubMed: 12499390]

Highlights

- *Shroom3* is expressed within cardiomyocytes and cardiac neural crest cells of the embryonic heart during important stages of cardiac development

- SHROOM3 loss-of-function leads to previously unreported cardiac defects in addition to neural tube, gut, kidney and lens defects

- SHROOM3 has a role during cardiac development as an actomyosin effector downstream of PCP signaling and is a novel contributor to cardiac development and CHD
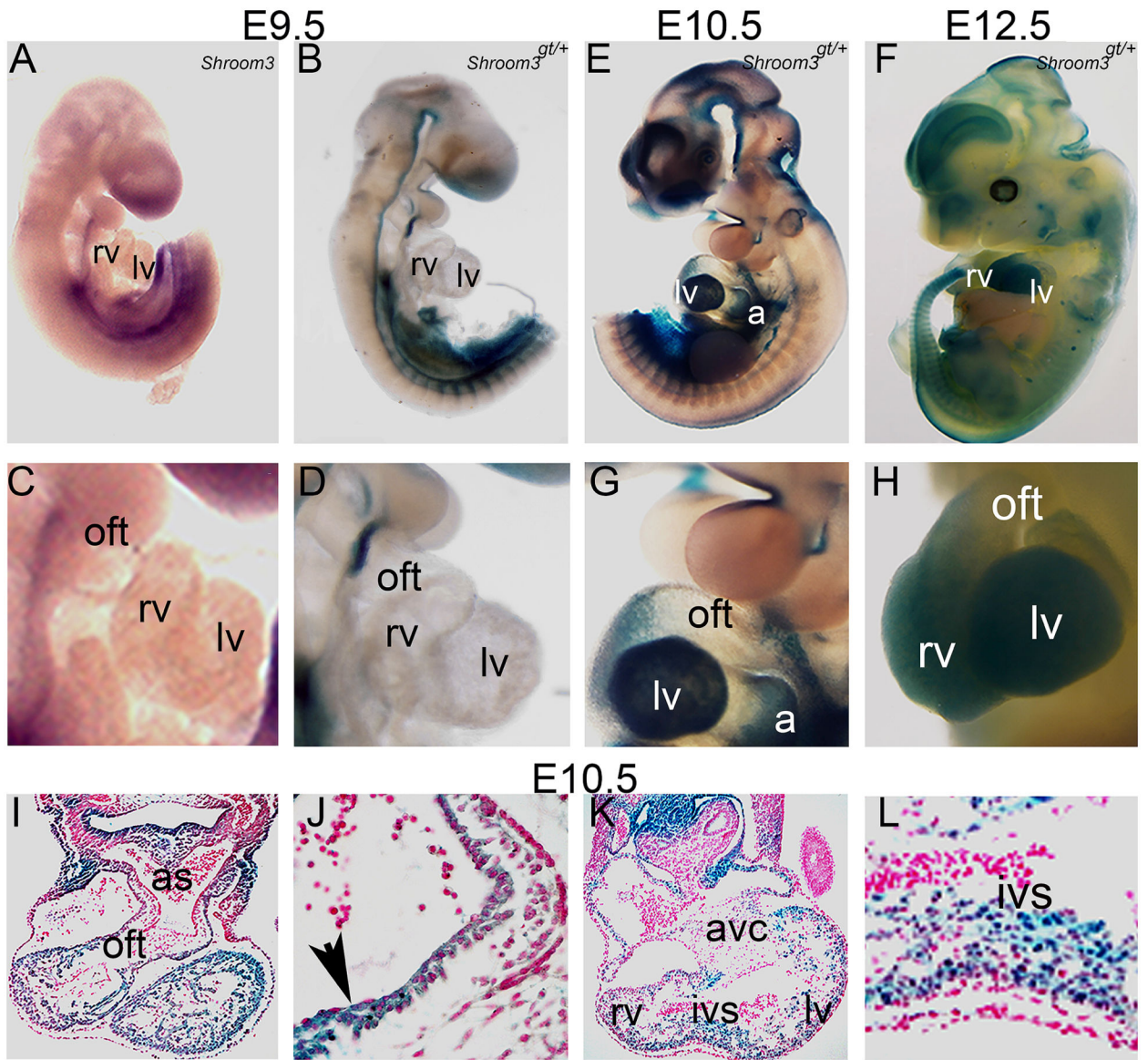
E9.5 E10.5 E12.5

Fig. 1.

Shroom3 is expressed in the heart during cardiac development

Spatiotemporal expression of *Shroom3* during cardiac development by WISH and β-galactosidase expression via X-gal staining from heterozygous *Shroom3*[+/gt] embryos, in whole mount and in section. WISH (A) and whole-mount X-gal staining (B, E, and F) at E9.5–12.5 (with magnification of the heart (C, D, G and H). Sections of E10.5 hearts (I–L). *Shroom3* expression pattern is consistent by WISH (A and C) and by β-galactosidase staining (B and D). *Shroom3* expression is present as previously reported in the neural tube, gut, mandibular arch and limbs (A, B, E and F). In whole mount E9.5 embryos, *Shroom3* expression is detected within the facial region of the head, lateral mesoderm and splanchnic mesoderm just dorsal to the cardiac outflow tract (A–D). At E10.5 and E12.5 *Shroom3* is detected in the four chambers of the heart (E–H) and in the OFT. In sections from X-gal staining, expression is evident in the OFT (I with magnification in J, and *Shroom3* OFT

expression indicated by an arrow in J), in both atria and in both ventricles (K and L). *Shroom3* expression is detected in the population of cells forming the aortic sac and in the splanchnic mesoderm (I and J). (as, aortic sac; ht, heart; ivs, intraventricular septum; lv, left ventricle; oft, outflow tract; rv, right ventricle).
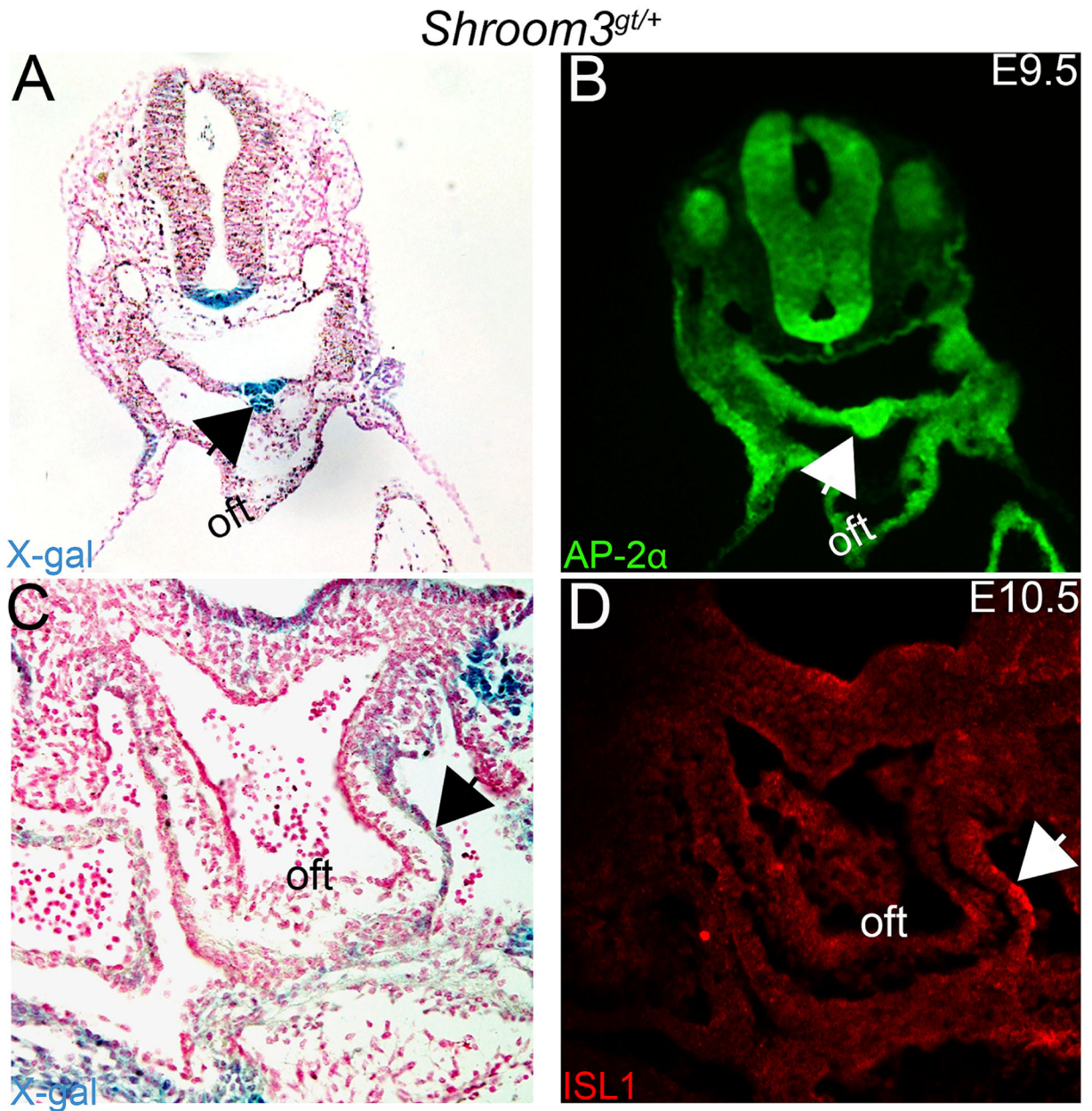
Shroom3^{gt/+}

Fig. 2.
Shroom3 is expressed within second heart field cells and cardiac neural crest cells
Shroom3 is expressed in cardiac neural crest cells and second heart field cells as indicated by overlapping *β-galactosidase* expression via X-gal staining and immunofluorescence by immunohistochemistry analysis. Serial sections of E9.5 *Shroom3^{+/gt}* embryos (A and B) demonstrate overlapping expression of *Shroom3* by X-gal staining (A) and immunofluorescence for cardiac neural crest cell marker AP-2α (B) within the developing aortic sac. Serial transverse sections of E10.5 *Shroom3^{+/gt}* embryos at the level of the developing outflow tract demonstrates overlapping expression of *Shroom3* by X-gal staining (C) and immunofluorescence for second heart field marker ISL1 (D). (oft, outflow tract.)
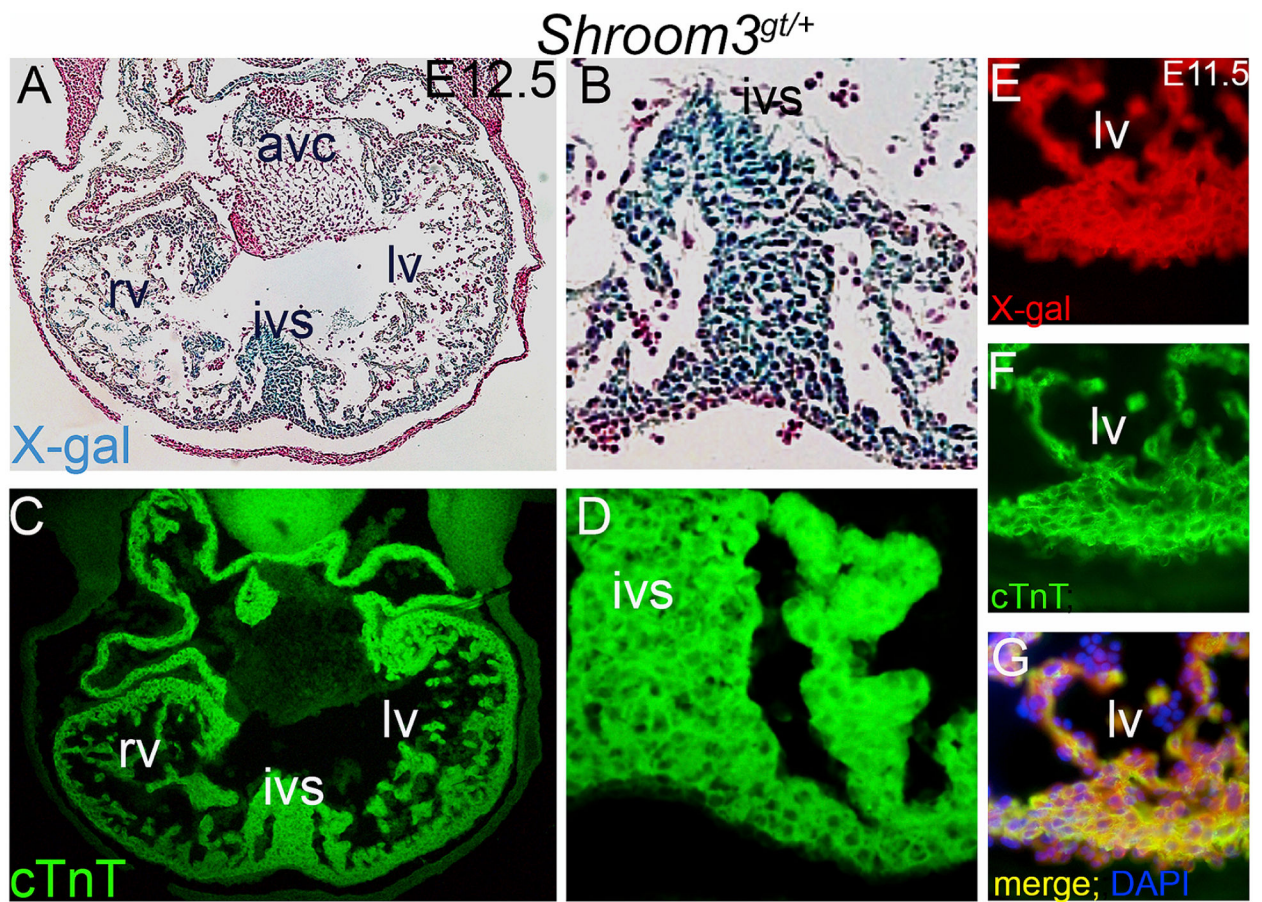
Fig. 3.

Shroom3 is expressed within cardiomyocytes

Shroom3 is expressed in cardiomyocytes, indicated by *β-galactosidase* expression via X-gal staining and immunofluorescence by immunohistochemistry analysis. E12.5 *Shroom3*[+/gt] embryo serial sections (A–D) demonstrate *Shroom3* expression detected by X-gal staining (A and B) in cardiomyocytes of the left ventricle and intraventricular septum, which also demonstrate immunofluorescence for cardiac troponin (C and D). E11.5 *Shroom3*[+/gt] embryo, left ventricular wall cryosections (E–G), demonstrate colocalization of immunofluorescence for X-gal (E) and immunofluorescence for cardiac troponin (F and G).
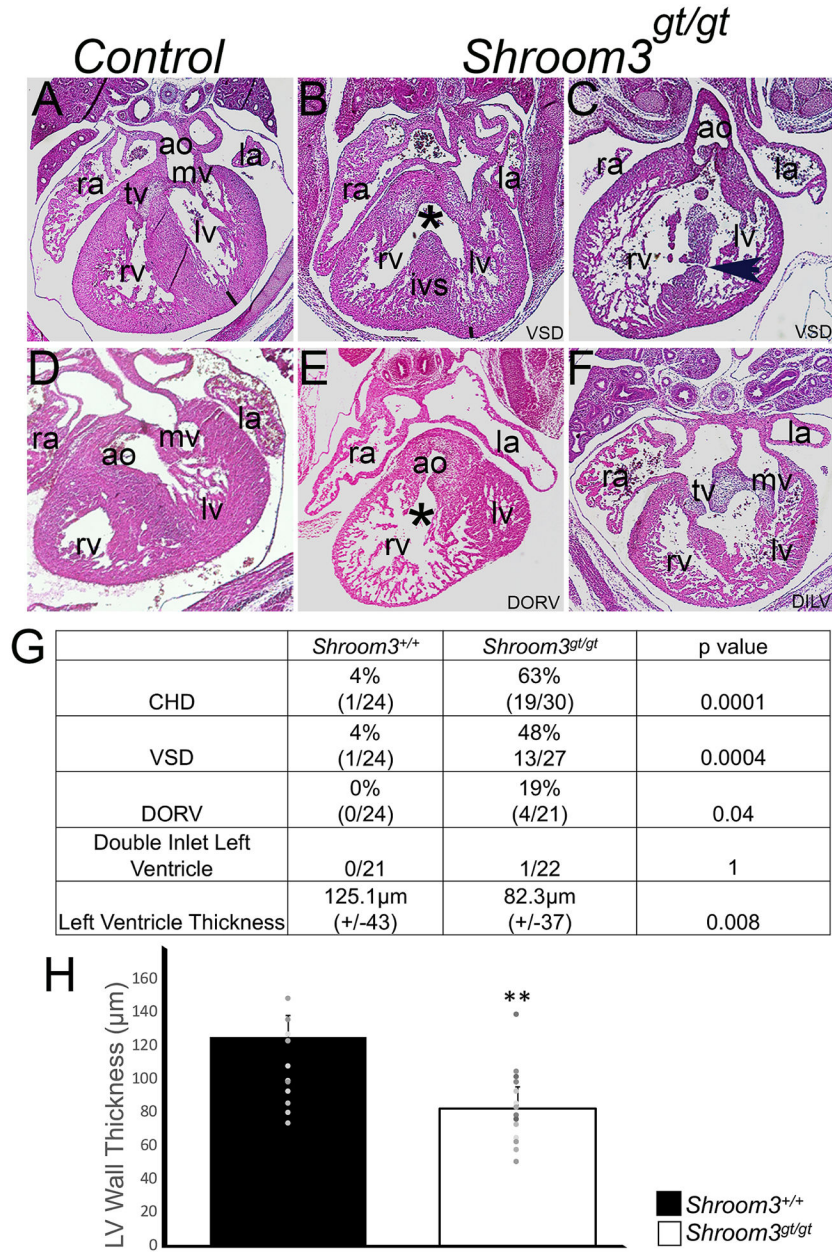
Fig. 4.

Shroom3^gt/gt mice exhibit cardiac defects

Transverse sections of hearts stained with H&E in *Shroom3^+/+* littermate controls (A and D) and *Shroom3^gt/gt* embryos with indicated heart defects (B, C, E and F). Frequency of identified heart defects (G) and left ventricular measurements (H). *Shroom3^+/+* littermate controls have normal cardiac structures (A and D). *Shroom3^gt/gt* embryos display CHDs (63%; p=0.0001 [B, C, E and F]). *Shroom3^gt/gt* mice have ventricular septal defects (VSD) (48%; p=0.0004), with membranous VSD (indicated by an asterisk in B) and muscular VSD (indicated by an arrowhead in C); and double outlet right ventricle, in which both the aorta (E) and pulmonary artery arise from the right ventricle (19%; p=0.04). In contrast *Shroom3^+/+* littermate controls (A and D) have a complete ventricular septum and the aorta

arises from the left ventricle and the pulmonary artery from the right ventricle. A single *Shroom3*$^{gt/gt}$ embryo with double inlet left ventricle (F), with both the left atrium and mitral valve and right atrium and tricuspid valve emptying into the left ventricle, was identified. *Shroom3*$^{gt/gt}$ mice exhibit ventricular thinning in the left ventricular compact myocardium. Mean lv wall thickness measurements in (H) with measurements represented by a black line in panel (A) and (B) (125.0±43μm, 82.0±37μm; p=0.008) shown. Measurements of the left ventricle were made by capturing images of transverse sections of E14.5 hearts from *Shroom3*$^{gt/gt}$ and *Shroom3*$^{+/+}$ littermate control embryos, then selecting a matching plane of section which included a 4-chamber view of the heart. The compact myocardium was measured at the lowest point of the left ventricular wall where it meets the ventricular septum. We compared *Shroom3*$^{gt/gt}$ hearts and *Shroom3*$^{+/+}$ littermate control hearts using Fisher's two-sided t-test for statistical analysis. A difference in denominator between groups reflects histologic section availability due to technical determinants. (ao, aorta; DILV, double inlet left ventricle; DORV, double outlet right ventricle; la, left atrium; lv, left ventricle; mv, mitral valve; pa, pulmonary artery; ra, right atrium; rv, right ventricle; tv, tricuspid valve; ivs, intraventricular septum.)
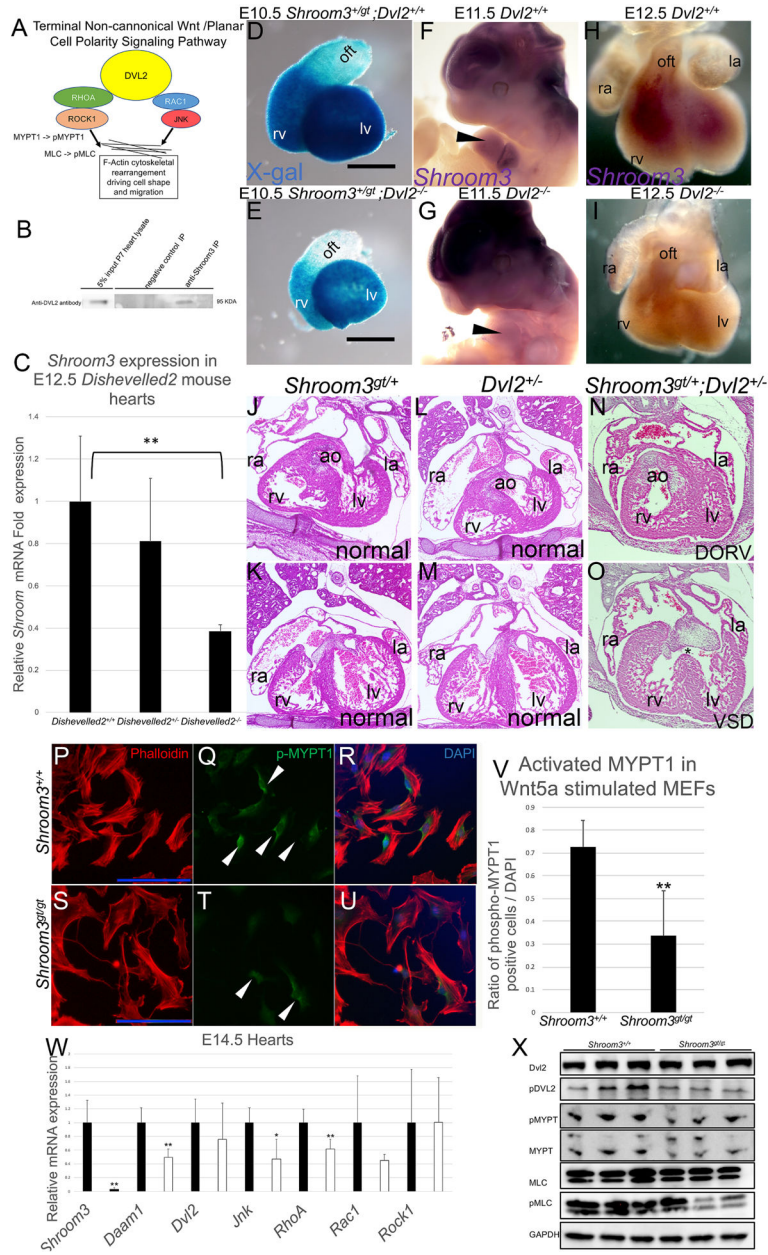
Fig. 5.

Shroom3 interacts with and is downstream of key planar cell polarity component *Dishevelled2* and SHROOM3 loss impacts planar cell polarity components

A schematic of PCP signaling (A), a Co-IP immunoblot demonstrating SHROOM and DVL2 physically interact within the heart (B), *Dvl2* transcriptionally regulates *Shroom3* demonstrated by gene expression analysis (C), X-gal (D–E) and WISH analysis (F–I) and H&E stained transverse heart sections demonstrating *Shroom3* and *Dvl2* genetic interaction (J–O). PCP signaling activation by immunofluorescence in cell culture (P–V), gene expression analysis (W) and proteins by immunoblot analysis (X) in embryo hearts. (A) Planar cell polarity pathway terminal components including, key cytoplasmic component DVL2, and terminal effectors, RAC1, JNK, RHOA and ROCK1, which phosphorylates

MLC and MYPT1, driving Actomyosin cytoskeletal rearrangement and subsequent changes in cell shape and movement. (B) SHROOM3 and DVL2 physically interact in the heart, demonstrated by Co-IP immunoblot, with DVL2 detected within P7 mouse heart lysate, pulled down using SHROOM3 antibody bound to agarose beads. (C) Expression analysis of *Shroom3* by RT-qPCR analysis in *Dvl2*$^{+/+}$*, Dvl2*$^{+/-}$ and *Dvl2*$^{-/-}$ hearts at E12.5 (n=5 of each genotype). In *Dvl2*$^{-/-}$ mouse hearts, there is a 60% reduction in *Shroom3* expression (p=0.03.) Analysis of *Shroom3* tissue specific expression pattern within the heart demonstrated a global reduction in *Shroom3* expression, demonstrated by comparing *Dvl*$^{+/+}$ and littermate *Dvl2*$^{-/-}$embryos by both X-gal staining (D and E) and WISH for *Shroom3* (F–I). *Shroom3* interacts genetically with *Dvl2* during cardiac development, demonstrated in crosses of *Shroom3*$^{+/gt}$ and *Dvl2*$^{+/-}$ mice, with histologic analysis of H&E stained transverse heart sections of embryos after ventricular septation at E14.5. OFT and ventricular septum in heterozygous *Shroom3*$^{+/gt}$(J and K) and *Dvl2*$^{+/-}$(L and M) embryos are phenotypically normal, whereas a littermate compound heterozygous *Shroom3*$^{+/gt}$;*Dvl2*$^{+/-}$ embryo has PCP associated cardiac defects DORV (N) and membranous VSD (O, asterisk) (n=76). (P–V) Mouse embryonic fibroblasts (MEF) were subjected to a scratch wound, treated with Wnt5a recombinant protein and 24 hours later analyzed by immunofluorescence. We imaged the scratch wound area, capturing cells having moved into the wound area, and quantified total cells, positive for phalloidin (P), as well as cells with positive immunofluorescence for activated MYPT1 within the cytoplasm (Q), in the entirety of each 1mm^2 visual field and calculated a ratio of MYPT1 positive cells over phalloidin positive cells (V). Compared with *Shroom3*$^{+/+}$ MEFs, *Shroom3*$^{gt/gt}$ MEFS have a significantly reduced ratio of activated MYPT1 positive cells (0.73 versus 0.33, standard deviation 0.11 and 0.19, p=0.02; averages of 4 different scratch wound areas with an average of 18 cells per area from (n=4) *Shroom3*$^{+/+}$ and (n=3) *Shroom3*$^{gt/gt}$ littermate embryos). (W) Expression analysis of PCP signaling pathway genes by RT-qPCR of *Shroom3*$^{gt/gt}$ mouse hearts and *Shroom3*$^{+/+}$ littermate control hearts at E12.5 (n=3–5 of each genotype). In *Shroom3*$^{gt/gt}$ mouse hearts, there is a statistically significant reduction in the expression of multiple PCP components (*Daam1, JNK, Rho*, and a trend towards decreased expression of *Rock1* and *Rac1*). P-values are calculated directly from mean dCq values and error bars represent standard deviation calculated from mean dCq values as a ratio of mean to total exponential values. (X) Immunoblot analysis of whole heart lysates from E12.5 and E14.5 *Shroom3*$^{+/+}$ and *Shroom3*$^{gt/gt}$ littermates. Activation of PCP represented by activated, phosphorylated, PCP central component DVL2 as well as terminal components MYPT1 and MLC, as compared to total protein. *Shroom3*$^{gt/gt}$ hearts exhibit observable reductions in PCP proteins and terminal components including phosphorylated MYPT1, phosphorylated MLC (pMLC), and phosphorylated DVL2 (pDVL2). (ao, aorta; co-immunoprecipitation assay, CoIP; ivs, intraventricular septum; la, left atrium; lv, left ventricle; oft, outflow tract; ra, right atrium; rv, right ventricle).
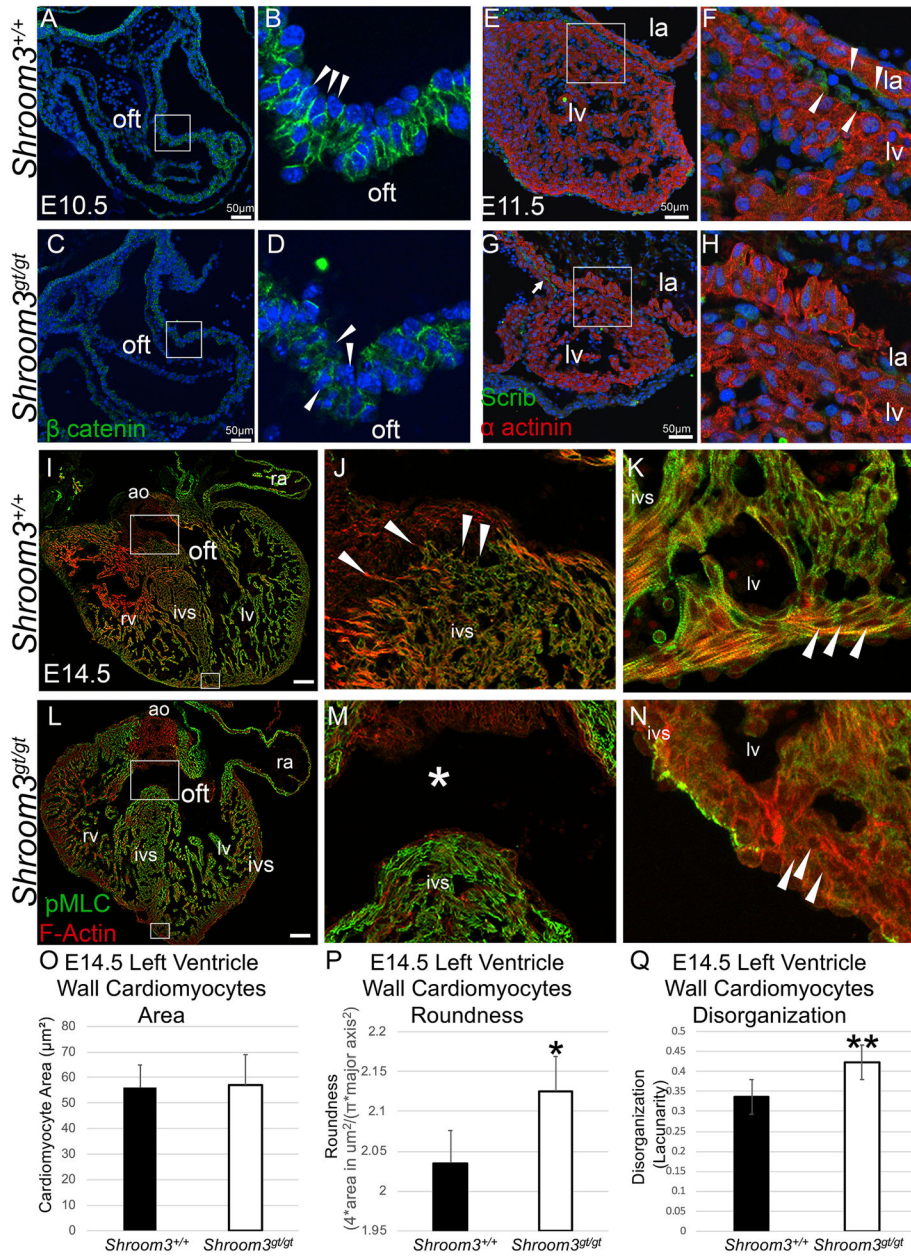
Fig. 6.

Shroom3[gt/gt] hearts have disrupted cardiomyocyte polarity, organization and morphology Cardiomyocyte polarity, organization and morphology measured with immunofluorescence analysis within the OFT and lv of E10.5, E11.5 and E14.5 hearts. Immunofluorescence analysis of adherens-junction component β-catenin in the OFT of E10.5 *Shroom3*^{+/+} (A–B) and littermate *Shroom3*[gt/gt] embryos (C–D), with further magnification of boxed sections (A and C) in (B and D), showing abnormal structure of the OFT membrane. In the *Shroom3*^{+/+} OFT membrane (B), cells are organized and aligned, with β-catenin localized to adheres junctions (white arrowheads). The *Shroom3*[gt/gt] OFT membrane (D) cells are disorganized with loss of β-catenin localization at the adherens junctions (white arrowheads). Immunofluorescence analysis of basolateral membrane marker SCRIB and cardiomyocyte

marker sarcomeric α-actinin (α-actinin) in the lv wall of E11.5 *Shroom3*^{+/+} (E–F) and littermate *Shroom3*[gt/gt] embryos (G–H), with further magnification of boxed sections (E and G) in (F and H), showing abnormal structure of the lv wall. The lv wall of *Shroom3*^{+/+} mice is compact and organized with well aligned cells and Scribble localized at the basolateral membrane of the epicardium (F, arrowhead). Whereas *Shroom3*[gt/gt] lv wall cardiomyocytes are disorganized and less compact with more space between cells, and without evident SCRIB at the ventricle epicardium basolateral membrane, though still evident in the basolateral membrane within the unaffected atria (G, arrow). F-actin and pMLC immunofluorescence analysis of hearts from E14.5 *Shroom3*^{+/+} (I) and littermate *Shroom3*[gt/gt] embryos (L), with further magnification of boxed sections showing abnormal structure of the membranous ventricular septum (J and M) and lv wall (K and N). In the *Shroom3*^{+/+} ventricular septum (J), lamellipodia and filopodia are visible, indicated with white arrows. The *Shroom3*[gt/gt] septum (M) cardiomyocytes are rounded, lacking lamellipodia and filopodia, and a membranous VSD is evident, indicated by an asterisk. The left ventricular wall of *Shroom3*^{+/+} mice is comprised of mature, elongated cardiomyocytes (K). We quantified cardiomyocyte area (O), roundness (P) and disorganization (Q) in *Shroom3*[gt/gt] and *Shroom3*^{+/+} littermate control embryos. We demonstrate that, compared to *Shroom3*^{+/+} littermate controls, *Shroom3*[gt/gt] embryo cardiomyocytes are the same size (56.1 μm^2 vs 57.1 μm^2, standard deviation= 8.8 and 11.9, p=0.9), but are more round (roundness 2.0 versus 2.1 (roundness=4*area in $\mu m^2/(\pi * major\ axis^2)$, standard deviation= 0.04 and 0.04, p=0.04) and less compact-more disorganized (lacunarity 0.33 versus 0.42, standard deviation= 0.04 and 0.03, p=0.04). (ao, aorta; ivs, intraventricular septum; la, left atrium; lv, left ventricle; oft, outflow tract; ra, right atrium; rv, right ventricle).
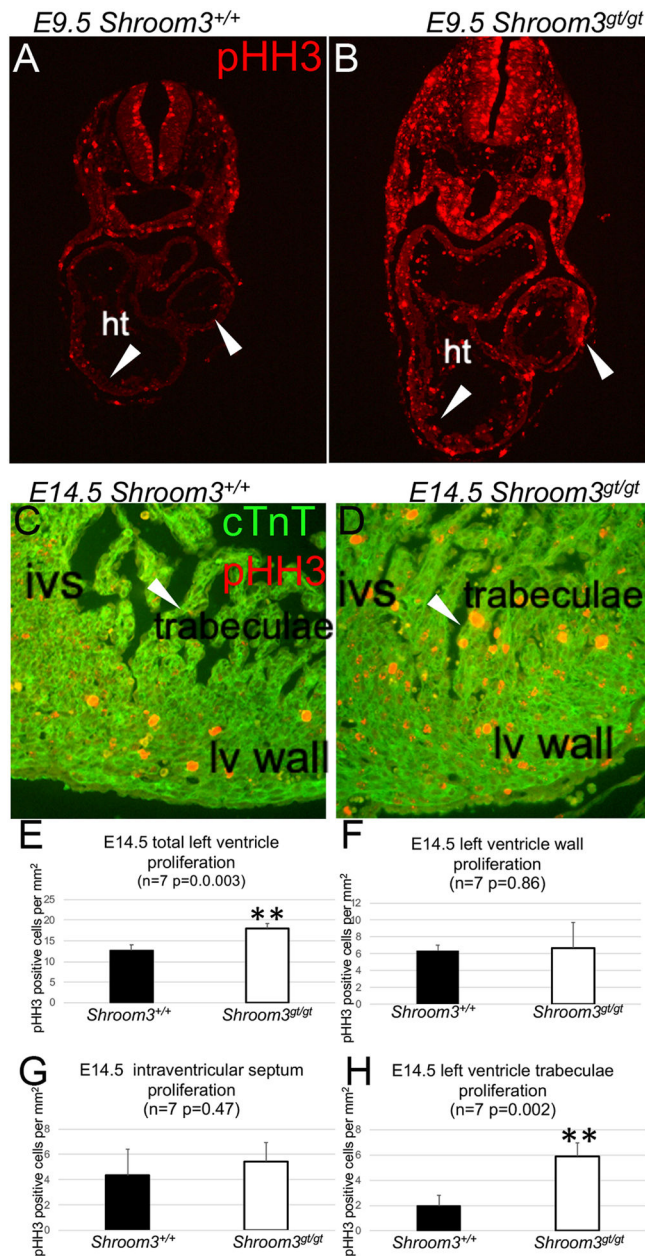
Fig. 7.

Shroom3^gt/gt hearts have increased left ventricular cardiomyocyte proliferation Immunofluorescence analysis of proliferation in E9.5 (A and B) and E14.5 embryos (C and D) with quantification (E–H). Immunofluorescence analysis of proliferation marker pHH3, in E9.5 *Shroom^+/+* embryos (A) and littermate *Shroom3^gt/gt.* embryos (B), demonstrating increased proliferation in *Shroom3^gt/gt* embryos (B). Immunofloresence analysis of pHH3 and cTnT to identify cardiomyocytes in the left ventricle, in matching transverse sections of E14.5 *Shroom^+/+* mice (C) and littermate *Shroom3^gt/gt* embryos (D), again demonstrating increased proliferation in *Shroom3^gt/gt* embryos (D). We quantified all positive cardiomyocytes (positive for pHH3 and cTnT) in the entire 1mm^2 visual field (E–H). *Shroom3^gt/gt* embryos have significantly increased cardiomyocyte proliferation within the

left ventricle (E) (12 versus 18 pHH3 positive cardiomyocytes per mm^2, standard deviation=1.3 and 1.2, p=0.003). *Shroom3$^{gt/gt}$* mice have increased proliferation localized to the ventricular trabeculae (1.9 versus 5.8 pHH3 positive cardiomyocytes per mm^2, standard deviation=0.8 and 1.0, p=0.002), whereas cardiomyocyte proliferation was equal within the left ventricle wall and ventricular septum (lv wall; 6.3 versus 6.6 pHH3 positive cardiomyocytes per mm^2, standard deviation=0.6 and 3.0, p=0.8) (septum; 4.3 versus 5.4 pHH3 positive cardiomyocytes per mm^2, standard deviation=0.8 and 1.0, p=0.47) (ht, heart; ivs, intraventricular septum; lv, left ventricle).

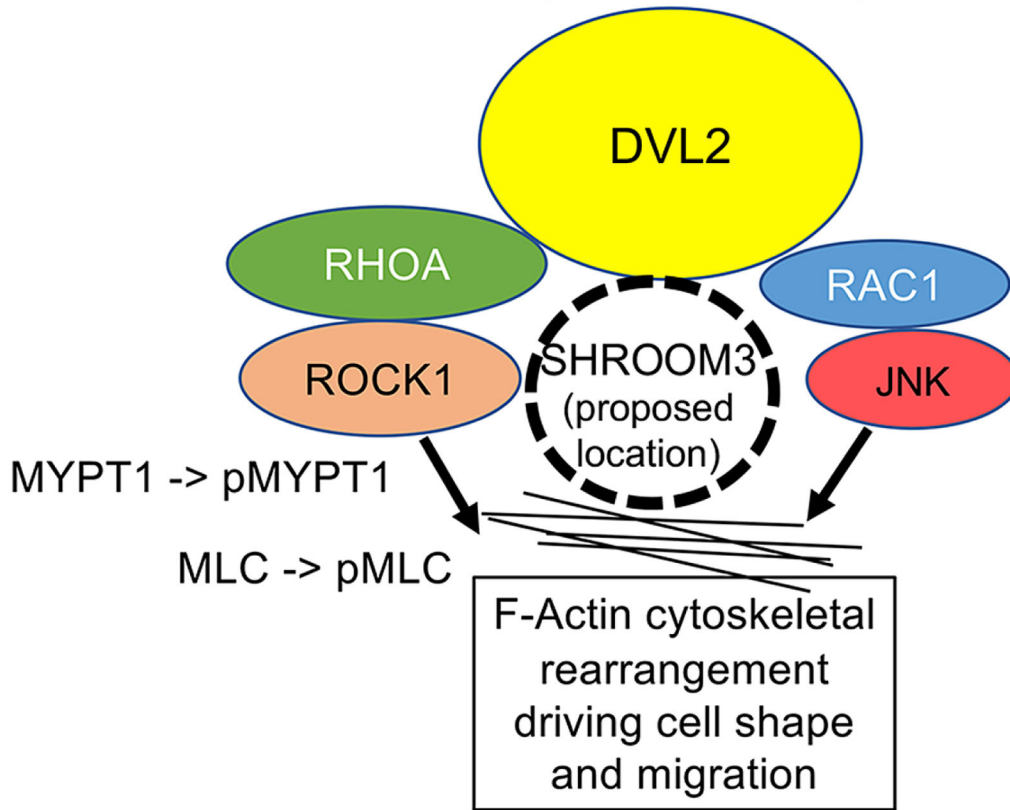# Terminal Non-cannonical Wnt /Planar Cell Polarity Signaling Pathway

Fig. 8.
Proposed location of SHROOM3 within the Wnt Signaling/ Planar Cell Polarity (PCP) pathway

A schematic of the noncanonical Wnt signaling/PCP pathway is shown with a proposed location of SHROOM3, based on these data and previous studies, in which SHROOM3 binds DVL2 and ROCK1 and functions with PCP's terminal actomyosin effectors.